Constraints on primordial magnetic fields from CMB distortions in the axiverse

Hiroyuki Tashiro, Joseph Silk, David J. E. Marsh

PHYSICAL REVIEW D **88,** 125024 (2013)

Constraints on primordial magnetic fields from CMB distortions in the axiverse

Hiroyuki Tashiro
Physics Department, Arizona State University, Tempe, Arizona 85287, USA

Joseph Silk
Institut d'Astrophysique, UMR 7095 CNRS, Université Pierre et Marie Curie, 98bis Boulevard Arago, 75014 Paris, France

Department of Physics and Astronomy, The Johns Hopkins University, Homewood Campus, Baltimore, Maryland 21218, USA and Beecroft Institute of Particle Astrophysics and Cosmology, Department of Physics, University of Oxford, Oxford OX1 3RH, United Kingdom

David J. E. Marsh
Perimeter Institute, 31 Caroline Street North, Waterloo, Ontario N2L 6B9, Canada
(Received 3 September 2013; published 26 December 2013)

Measuring spectral distortions of the cosmic microwave background (CMB) is attracting considerable attention as a probe of high energy particle physics in the cosmological context, since primordial inflation explorer (PIXIE) and polarized radiation imaging and spectroscopy mission (PRISM) have recently been proposed. In this paper, CMB distortions due to resonant conversions between CMB photons and light axionlike particles (ALPs) are investigated, motivated by the string axiverse scenario which suggests the presence of a plenitude of light axion particles. The distortions due to resonant conversions have a frequency-independent shape, in contrast to μ and y distortions. Therefore, one can distinguish the distortions due to resonant conversions from μ and y distortions. Since these resonant conversions depend on the strength of primordial magnetic fields, constraints on CMB distortions can provide an upper limit on the product of the photon-ALP coupling constant g and the comoving strength of primordial magnetic fields B. Potentially feasible constraints from PIXIE/PRISM can set a limit $gB \lesssim 10^{-16}$ GeV^{-1} nG for ALP mass $m_\phi \lesssim 10^{-14}$ eV. Although this result is not a direct constraint on g and B, it is significantly tighter than the product of the current upper limits on g and B.

DOI: 10.1103/PhysRevD.88.125024 PACS numbers: 14.80.Va, 98.70.Vc

I. INTRODUCTION

An axion is a strongly motivated particle for a dark matter candidate. The axion was originally introduced to solve the strong CP problem in quantum chromodynamics (QCD) [1–3]. Axionlike particles (ALPs) also appear naturally in string theory [4,5]. The topological complexity of string theory compactifications can provide a plenitude of light ALPs spanning many orders of magnitude in mass, known as the string axiverse scenario [6–8]. In principle there is no lower limit to the ALP mass in this scenario, though the lower limit of relevance for dark matter is the Hubble scale $H_0 \approx 10^{-33}$ eV.

Recent gamma-ray data from blazars suggests the existence of cosmological magnetic fields stronger than 10^{-16} G in large voids [9,10]. Such magnetic fields can be accounted for by primordial magnetic fields, which are generated in the early Universe (for recent reviews, see Refs. [11–13]). Since ALPs generally couple with electromagnetic fields, one can expect a conversion between cosmic microwave background (CMB) photons and ALPs in the presence of primordial magnetic fields. Such a conversion produces observable distortions in the CMB spectrum [14]. Reference [15] has studied the resonant conversion between CMB photons and ALPs. The resonant conversion generates the frequency-independent deficit distortions from the blackbody spectrum, which are totally different from CMB distortions due to thermal injections in the early Universe called as μ and y distortions [45].

They obtained the photon-ALP mixing constraint from the Far Infrared Absolute Spectrophotometer (FIRAS) data of the Cosmic Background Explorer (COBE) [16,17]. Since the COBE FIRAS constraint on the resonant conversion probability P corresponds to $P < 5 \times 10^{-5}$, they provided a constraint $gB < 10^{-13}$–10^{-11} GeV^{-1} nG for ALP masses between 10^{-14} and 10^{-4} eV, where g is the coupling constant and B is the spatially averaged magnetic field strength at the present epoch. Their result suggests that, if primordial magnetic fields have a strength close to the current upper limit, the CMB distortion constraint gives a stronger constraint on g than the solar and astrophysical bounds [18–20].

Recently, PIXIE [21] and PRISM [22] have been proposed to provide precision measurements of the CMB

frequency spectrum. Measuring CMB distortions from the blackbody spectrum is a good probe to access the thermal history of the Universe [23–27] (see Refs. [28,29] for recent reviews). The current goal of these sensitivities to CMB distortions is set to be a factor $\sim 10^4$ improvement on the COBE FIRAS. Here, we revisit CMB distortions due to resonant photon-ALP conversions and make a forecast about the feasibility of future constraints from PIXIE/PRISM. Because distortions due to resonant conversion have a different spectral shape from μ and y distortions, which are generated by thermal injections in the early Universe, one can distinguish distortions by resonant conversion from μ and y distortions. We also expand the constraint to smaller ALP masses, $< 10^{-14}$ eV, than in Ref. [15]. Such small-mass ALPs naturally arise in the axiverse scenario and have diverse phenomenology in the CMB, large-scale structure, and black hole astrophysics that can constrain them independently of their couplings to the visible sector [30–34]. However, when the coupling to photons is present such ALPs can go through resonant conversions with CMB photons due to plasma effects in the cosmic dark age and be constrained independently of their contribution to dark matter. We evaluate CMB distortions due to small-mass ALPs, taking into account multiple resonant conversions.

This paper is organized as follows. We briefly review the resonant conversion between photons and ALPs in the cosmological scenario in Sec. II. We also derive the analytical form of the resonant conversion in both strong and weak coupling limits at the resonant epoch. In Sec. III, we calculate the resonant conversion probability numerically and evaluate the PIXIE/PRISM constraints on the ALP coupling and primordial magnetic field strength. Section IV is devoted to our conclusions. Throughout this paper, we adopt natural units where $\hbar = 1$, $c = 1$ and the Boltzmann constant $k_B = 1$. We use cosmological parameters for a flat ΛCDM model: $h = 0.69$, $\Omega_{\rm B}h^2 = 0.022$, and $\Omega_{\rm C}h^2 = 0.11$.

II. RESONANT CONVERSIONS

ALPs couple to electromagnetic fields through a two-photon vertex. In the existence of external magnetic fields, electromagnetic fields in the ALP interaction terms can be decomposed into the dynamical part of photons and the external magnetic field part. As a result, the interaction term of an ALP and a photon with external magnetic fields is given by

$$\mathcal{L} = g\omega B_T A_\parallel \phi, \tag{1}$$

where ω is the photon frequency, B_T is the component of the external magnetic field perpendicular to the propagation of photons, and $A_\parallel$ is the component of a photon parallel to the B_T component.

Because of this interaction, the propagation eigenstates of the photon-ALP system (γ, ϕ) are different from the interaction eigenstates with external magnetic fields. Therefore, conversion between γ and φ occurs in the same way as for massive neutrinos of different flavors. The mixing angle of (γ, ϕ) in vacuum is given by [35]

$$\cos 2\theta_{\rm v} = \frac{m_\varphi^2}{\sqrt{(2gB_T\omega)^2 + m_\phi^4}},$$
$$\sin 2\theta_{\rm v} = \frac{2gB_T\omega}{\sqrt{(2gB_T\omega)^2 + m_\phi^4}}, \tag{2}$$

where m_ϕ is the ALP mass. This mixing angle produces photon-ALP oscillations with a wave number

$$k = \frac{\sqrt{m_\phi^4 + (2gB\omega)^2}}{2\omega}. \tag{3}$$

In the cosmological plasma, the photon dispersion relation is modified due to plasma effects. This modification can be parametrized by an effective photon mass m_γ. Among the various plasma effects, the scatterings off free electrons and neutral atoms make negative and positive contributions to the effective photon mass, respectively. Because of these effects, the effective mass can be given as [36]

$$m_\gamma^2 = \omega_p^2 - 2\omega^2(n_{\rm H} - 1), \tag{4}$$

where ω_p is the plasma frequency $\omega_p^2 = 4\pi\alpha n_{\rm e}/m_e$ with the fine structure constant α, the electron mass m_e and the free electron number density $n_{\rm e}$. The refractive index of neutral hydrogen $n_{\rm H}$ is set to $(n_{\rm H} - 1) = 1.36 \times 10^{-4}$ under normal conditions [37]. In Eq. (4), we ignore the contributions of helium and magnetic fields, because these effects are negligibly small [36].

The effective photon mass depends on the evolution of the ionization fraction $x(z)$ through the neutral hydrogen and free electron number densities. Ionized hydrogen recombines with free electrons at $z \approx 1100$ and is reionized around $z \approx 10$ [38]. We calculate $x(z)$ with RECFAST [39], adopting a toy model for reionization which is given by a tanh function, $x(z) = 1 + \tanh[(z - z_{\rm re})/\Delta z]$ with $z_{\rm re} = 10$ and $\Delta z = 1$. We plot the evolution of the effective photon mass in Fig. 1 with CMB temperature T_0. The effective mass squared has positive and negative contributions from scattering off free electrons and neutral atoms, respectively. As a result, the effective mass becomes negative for high frequencies in the dark ages where negative contributions dominate positive ones.

The effective photon mass modifies photon-ALP oscillations through the Lagrangian. This effect arises as the effective mixing angle $\tilde{\theta}$ [40]:

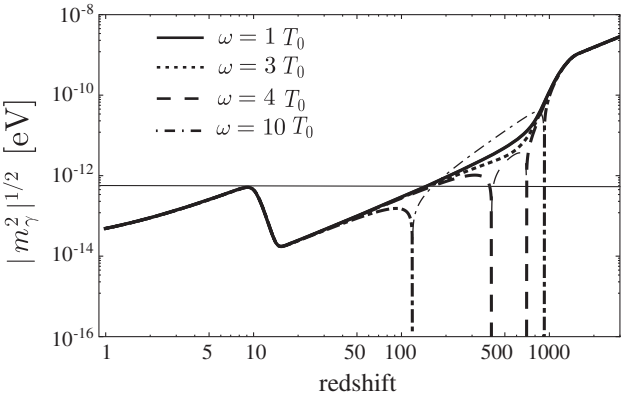

FIG. 1. The evolution of the effective photon mass. Thick lines represent positive effective mass regions, while thin lines show negative effective mass regions. The solid, dotted, dashed and dashed-dotted lines are for $\omega = T_0$, $3T_0$, $4T_0$ and $10T_0$, respectively, with CMB temperature T_0. For $\omega \lesssim 3T_0$ the photon mass is always positive and the minimum ALP mass that experiences resonant conversion is $m_\phi \approx 10^{-14}$ eV, with multiple resonance for $m_\phi \lesssim 10^{-12}$ eV (horizontal line). Since m_γ passes through zero and back for high ω, these will be most relevant for light ALPs and multiple resonances.

$$\cos\ 2\tilde{\theta} = \frac{\cos\ 2\theta_{\rm v} - \xi}{\sqrt{(\sin\ 2\theta_{\rm v})^2 + (\cos\ 2\theta_{\rm v} - \xi)^2}},$$
$$\sin\ 2\tilde{\theta} = \frac{\sin\ 2\theta_{\rm v}}{\sqrt{(\sin\ 2\theta_{\rm v})^2 + (\cos\ 2\theta_{\rm v} - \xi)^2}}, \quad (5)$$

where the parameter ξ controls the significance of the plasma effects:

$$\xi = \frac{m_\gamma^2}{\sqrt{m_\phi^4 + (2gB\omega)^2}} = \left(\frac{m_\gamma}{m_\phi}\right)^2 \cos\ 2\theta_{\rm v}. \quad (6)$$

As shown in Fig. 1, the effective mass at early Universe can be much larger than the ALP mass and $\xi \gg 1$. In this case, the conversion between γ and φ is suppressed. However, as the Universe evolves, the effective mass equals an ALP mass and ξ reaches unity. At this time, the effective mixing angle becomes $\pi/4$ and the resonant conversion occurs between photons and ALPs with this mass. This is in analogy to "resonant" neutrino oscillations known as the Mikheyev-Smirnov-Wolfenstein effect [41,42].

The conversion probability for the resonance is given by [43]

$$P \approx \frac{1}{2} + \left(p - \frac{1}{2}\right) \cos\ 2\theta_p\ \cos\ 2\theta_0, \quad (7)$$

where p is the level crossing probability and θ_p and θ_0 are the effective mixing angles at the photon production ($z \gg 1$) and detection points ($z = 0$), respectively. At the photon production point (i.e. at reheating), since the redshift is very high, ξ is large. Hence we approximate $\cos\ 2\theta_p \sim -1$ throughout this paper.

The level crossing probability p indicates the nonadiabaticity of the conversion. While p becomes zero in the limit of the adiabatic conversion, p reaches unity in the extremely nonadiabatic case. In order to obtain the level crossing probability, we make the approximation that m_γ varies linearly in the resonance regime and make a Taylor-series expansion at the resonance position, neglecting the second- and higher-derivative terms. In this approximation, the level crossing probability is given by applying the Landau-Zener result [43]:

$$p \approx \exp\left[-\frac{k_r r}{2}\frac{\sin^2 2\theta_r}{\cos\ 2\theta_r}\right], \quad (8)$$

where k_r and θ_r are, respectively, the oscillation wavelength and vacuum mixing angle at the resonance epoch, and r is a scale parameter to be evaluated at the location where a resonance occurs [36]:

$$r = \left|\frac{d\ \ln\ m_\gamma^2(t)}{dt}\right|^{-1}_{t=t_r}, \quad (9)$$

where t_r refers to the time at the resonance.

For small m_ϕ ($m_\phi < 10^{-12}$ eV), we expected from Fig. 1 that multiple resonances occur. The conversion probability can be calculated in a manner similar to the single resonance case. Following the classical probability result, we obtain the probability for the double resonant case by replacing p by $p_1(1-p_2) + p_2(1-p_1)$, where p_1 and p_2 are the probabilities for the first and second resonances, respectively [43]. Similarly to the double resonant case, the probability for more multiple resonances can be calculated.

Resonant photon-ALP conversions depend on the component of external magnetic fields perpendicular to the propagation direction of photons, B_T. Generally, primordial magnetic fields have structures which depend on the generation mechanisms of these fields. Therefore, the resonant conversion probability is possibly anisotropic due to these structures and depends on the ratio of the magnetic field coherent scale to the resonant scale. In this paper, we focus on the monopole component of CMB distortions to the blackbody spectrum.

Before calculating resonant conversion probabilities numerically, it is worth estimating them analytically for two cases: $m_\varphi \gg m_{\gamma 0}$ and $m_\varphi \ll m_{\gamma 0}$, where $m_{\gamma 0}$ is the effective photon mass at the detection point ($z = 0$).

In the case of $m_\varphi \gg m_{\gamma 0}$, the resonant conversion probability has been studied in Ref. [15]. The mixing angle at the detection point is expressed by that in the vacuum state given by Eq. (2). Since we are interested in the weak mixing limit $g\langle B_0^2\rangle^{1/2}\omega \ll m_\varphi^2$, we can approximate $\cos\ 2\theta_0 \approx 1$. In this case, the resonant conversion happens only once.

Therefore the conversion probability is provided by Eq. (7), and the sky-averaged conversion probability can be approximated by

$$\langle P\rangle \approx 1 - p. \tag{10}$$

In order to satisfy the COBE FIRAS limit $\langle P\rangle < 5\times 10^{-5}$, a strong nonadiabatic resonance $p \sim 1$ is required. For the single resonance case, p is given by Eq. (8). A strong nonadiabatic condition, $p \approx 1$, leads the level crossing probability to

$$p \approx 1 - \frac{k_r r}{2}\frac{\sin^2 2\theta_r}{\cos 2\theta_r}. \tag{11}$$

Accordingly, in the weak coupling limit, the conversion probability at a comoving frequency ω can be provided by [15]

$$\langle P\rangle \approx \pi r\omega \frac{g^2\langle B_0^2\rangle (1+z_r)^5}{m_\phi^2}, \tag{12}$$

where the redshift factor comes from the dependence of both magnetic fields and CMB physical frequency on the resonant epoch.

For 10^{-14} eV $< m_\varphi < 5\times 10^{-13}$ eV, CMB photons suffer multiple resonances. Since photons are still detected in vacuum, we can approximate $\cos 2\theta_0 \approx 1$ in the weak mixing limit. For the double resonance case, the sky-averaged conversion probability is expressed as

$$\langle P\rangle \approx 1 - p_1(1-p_2) - p_2(1-p_1). \tag{13}$$

It is clear that the COBE FIRAS limit requires fine-tuning of p_1 and p_2. Accordingly, for 10^{-14} eV $< m_\varphi < 5\times 10^{-13}$ eV, the parameter regions of g and $\langle B^2\rangle^{1/2}$ are tightly restricted.

In the case of $m_\varphi \ll m_{\gamma 0}$, photons are no longer detected in vacuum, and the mixing angle at the detection point is given by Eq. (5). Therefore, $\cos 2\theta_0$ is approximated by $\cos 2\theta_0 \sim -1$ in the weak mixing limit. Then, the sky-averaged probability for the resonant conversion can be written as

$$\langle P\rangle \approx p. \tag{14}$$

For low frequencies ($\omega < 4T_0$), the effective photon mass is always positive and larger than the ALP mass. Therefore, there is no resonance and the photon-ALP conversion is adiabatic. This results in the sky-averaged probability for the resonant conversion being $\langle P\rangle = 0$ with $p = 0$. However, for high frequencies ($\omega \gtrsim 4T_0$), double resonant conversions happen. The sky-averaged probability for the resonant conversion is given by

$$\langle P\rangle \approx p_1(1-p_2) + p_2(1-p_1). \tag{15}$$

In the double resonant case, the COBE FIRAS limit requires strong nonadiabatic resonances, $p_1 \sim 1$ and $p_2 \sim 1$, or completely adiabatic conversions, $p_1 \ll 1$ and $p_2 \ll 1$. Here, we focus on only the case of strong nonadiabatic resonances. When the weak coupling limit is valid at the resonant epochs, the resonant conversion probability is given by

$$\langle P\rangle \approx \pi\omega \frac{g^2\langle B_0^2\rangle}{m_\phi^2}[r_1(1+z_1)^5 + r_2(1+z_2)^5], \tag{16}$$

where the subscripts 1 and 2 denote values at the first and second resonant epochs, respectively.

The magnetic field strength and CMB frequency at the resonant epochs depend on the redshift due to the cosmological expansion. As m_φ decreases, the weak coupling limit is no longer valid and the strong coupling limit $g\langle B_0^2\rangle^{1/2}\omega \gg m_\varphi^2$ is satisfied at the resonant epochs, although the weak coupling limit is still valid at the detection point ($z = 0$). We find that the level crossing probability in the strong coupling limit has the same approximate form as in the weak coupling limit (see also the Appendix). Accordingly, the sky-averaged conversion probability can be written as

$$\langle P\rangle \approx \pi\omega \frac{g^2\langle B_0^2\rangle}{m_\varphi^2}[r_1(1+z_1)^5 + r_2(1+z_2)^5]. \tag{17}$$

In both weak and strong coupling limits, the resonant conversion probability can be expressed in the same form as shown in Eqs. (16) and (17).

III. CMB DISTORTIONS AND CONSTRAINTS

A photon-ALP coupling causes resonant conversions of CMB photons to ALPs. In the standard big bang scenario, the CMB spectrum is predicted as a blackbody spectrum. When conversions happen after the decoupling of CMB thermal equilibrium, they can produce observable CMB distortions from the blackbody spectrum.

COBE FIRAS confirmed that the CMB spectrum is well fit to a blackbody spectrum at temperature $T_0 = 2.72548 \pm 0.00057$ K [44]. The intensity of the blackbody spectrum is given by

$$I_0(\omega) = \frac{\omega^3}{2\pi^2}[\exp(-\omega/T(z)) - 1]^{-1}. \tag{18}$$

Because of the presence of photon-ALP conversions, the observed intensity is modified to[1]

$$I_{\rm obs}(\omega) = I_0(\omega)(1 - P(\omega)). \tag{19}$$

[1]This equation is valid for ALP mass resonances occurring after the recombination epoch. When the resonant conversion happens before the recombination epoch, the distortion produced by the resonant conversion is modified, because CMB photons still couple with cosmic plasma. For a detailed analysis of this case, see Ref. [15].

Therefore, the sky-averaged CMB distortion from the blackbody spectrum can be written as

$$\frac{\Delta I(\omega)}{I_0(\omega)} = \frac{\langle I_{\rm obs}(\omega)\rangle - I_0(\omega)}{I_0(\omega)} = -\langle P(\omega)\rangle. \qquad (20)$$

We show the frequency dependence of the CMB distortions for different ALP masses and $g\langle B_0^2\rangle^{1/2}$ in Fig. 2. Note that, since the resonant conversion creates the deficit from the blackbody spectrum, the y axis denotes $-\Delta I/I_0$. In this figure, we use the frequency normalized to the CMB temperature T_0 and normalize m_φ and $g\langle B_0^2\rangle^{1/2}$ in units of eV and GeV^{-1} nG, respectively. For $m_\varphi = 10^{-10}$ eV, the resonant conversion happens only once. Both lines for $m_\varphi = 10^{-10}$ eV in Fig. 2 show that the conversion probability depends on $g^2\langle B_0^2\rangle$ and is proportional to ω. These are well described by Eq. (12).

On the other hand, for $m_\varphi = 10^{-16}$ eV, the number of resonant conversions depends on the CMB frequencies. While there is no resonant conversion at low frequencies $x < 4$, the resonance conversion occurs twice at high frequencies $x \gtrsim 4$. At both resonant epochs ($z > 100$), the strong coupling condition is satisfied for $g\langle B_0^2\rangle^{1/2} \gtrsim 10^{-4}$. Therefore, the resonant conversion probability can be written as Eq. (17). In Fig. 2, both lines for $m_\varphi = 10^{-16}$ eV show that the resonant conversion probability also depends on $g\langle B_0^2\rangle^{1/2}$ as expected from Eq. (17). The frequency dependence is not trivial, because the resonance epochs depend on the frequency as shown in Fig. 1. When we assume $z_1 > z_2$, we find that, although the magnetic field strength and CMB frequency are larger at higher redshift, the second term in Eq. (17) makes a dominant contribution. Figure 2 shows that, as the CMB frequency increases, $\langle P\rangle$ also becomes large on the high frequency side $\omega \gtrsim 5T_0$, similarly to the case of $m_\varphi > 10^{-10}$ eV where the conversion probability is proportional to the frequency.

CMB distortions are also created in the thermalization process of energy injections in the early Universe. Usually, these distortions are described by three types of distortions: μ- and y-type distortions [45] and an intermediate type between μ- and y-type distortions [46,47]

For comparison, in Fig. 2, we show the frequency dependence of μ- and y-type distortions. Here, we plot these distortions with COBE limits $\mu < -1.5 \times 10^{-5}$ and $y < 9. \times 10^{-5}$ [17]. Compared with these distortions, the resonant conversion creates frequency-independent distortions that make differences on high frequencies. Although μ-type distortions are suppressed and y-type provide excess distortions ($\Delta I/I_0 > 0$), the resonant conversion generates the deficit distortions.

Currently, PRISM is designed to measure the deviation $\Delta I_{\rm PRISM}(\omega) \approx 2 \times 10^{-26}$ $\mathrm{Wm}^{-2}\,\mathrm{Hz}^{-1}\,\mathrm{Sr}^{-1}$ for the CMB frequency range 30 GHz $< \omega <$ 1000 GHz ($0.5 < x < 17.5$) [22]. We adopt these values as the PIXIE/PRISM sensitivity for CMB distortions. We evaluate the PIXIE/PRISM constraints on the ALP coupling and magnetic fields $g\langle B_0^2\rangle^{1/2}$ from these values. We plot the PIXIE/PRISM constraint as functions of an ALP mass m_φ in Fig. 3.

COBE FIRAS has provided the best upper bound on possible CMB distortions from the blackbody spectrum. According to Ref. [17], we assume that COBE FIRAS constraint is $\Delta I_{\rm FIRAS}(\omega) < 3 \times 10^{-22}$ $\mathrm{Wm}^{-2}\,\mathrm{Hz}^{-1}\,\mathrm{Sr}^{-1}$ for frequencies $T_0 < \omega < 10T_0$ and evaluate the COBE FIRAS limit. For comparison, we show the COBE FIRAS limit as thin lines in Fig. 3.

For $m_\varphi > 10^{-12}$ eV, the resonant conversion occurs only once. The conversion probability can be written as Eq. (12) and is proportional to $g^2\langle B_0^2\rangle$. Therefore, as shown in Fig. 3, PIXIE/PRISM can give a much better constraint on

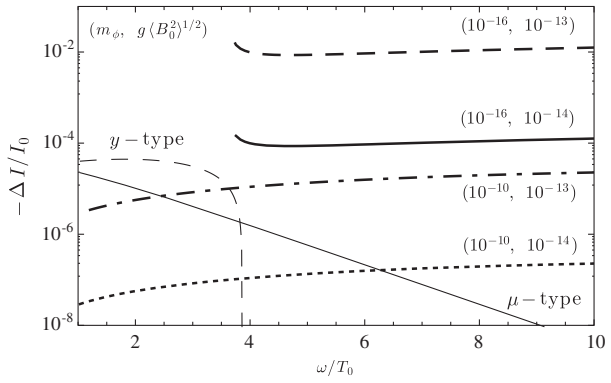

FIG. 2. Frequency dependence of the resonant conversion probability. The solid and dashed lines represent $g\langle B_0^2\rangle^{1/2} = 10^{-14}$ and 10^{-13} GeV^{-1} nG for $m_\phi = 10^{-16}$ eV, respectively. The dashed-dotted and dotted lines are for $g\langle B_0^2\rangle^{1/2} = 10^{-14}$ and 10^{-13} GeV^{-1} nG for $m_\phi = 10^{-10}$ eV, respectively. For comparison, we plot μ- and y-type distortions with COBE limits in thin solid and dashed lines, respectively. Resonance for masses $m \lesssim 10^{-14}$ eV only occurs for $\omega \gtrsim 4T_0$, as can be seen also in Fig. 1.

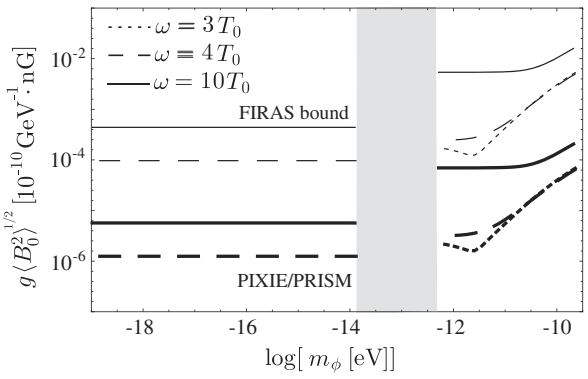

FIG. 3. Constraint on $g\langle B_0^2\rangle^{1/2}$ as functions of ALP mass m_φ. The thick lines are for the PIXIE/PRISM limit and the thin lines are for the COBE FIRAS limit. The dotted, dashed and solid lines represent frequencies $\omega = 3T_0$, $\omega = 4T_0$ and $\omega = 10T_0$, respectively. The mass region where fine-tuned $g\langle B_0^2\rangle^{1/2}$ is required to satisfy the COBE FIRAS limit is shown as the shaded region.

$g\langle B_0^2\rangle^{1/2}$ than COBE FIRAS and the improvement is roughly given by the ratio $\sqrt{\Delta I_{\rm PRISM}/\Delta I_{\rm FIRAS}} \sim 10^2$.

In the shaded region, the multiple resonances happen while the detection point ($z = 0$) is in vacuum, $m_\phi \gg m_{\gamma 0}$. The resonant conversion probability is provided by Eq. (13). As discussed above, the COBE constraint requires fine-tuned $g\langle B_0^2\rangle^{1/2}$. This means that ALPs in this mass region are effectively ruled out.

In the case of $m_\phi < 10^{-14}$ eV, there is no resonant conversion for lower frequencies $\omega < 4T_0$. The strong constraint on $g\langle B_0^2\rangle^{1/2}$ cannot be obtained for such low frequencies. On the other hand, CMB photons with higher frequencies $\omega \gtrsim 4T_0$ suffer double resonant conversions. As a result, the constraints on $g\langle B_0^2\rangle^{1/2}$ are divided to three ALP mass regions which correspond to Eqs. (16) and (17).

When $g\langle B_0^2\rangle^{1/2}$ attains the value of the PRISM/PIXIE constraint in Fig. 3, the weak coupling limit is valid at resonance epochs for $m \gtrsim 10^{-17}$ eV. The resonant conversion probability is given by Eq. (16). Although Eq. (16) has an explicit dependence on m_ϕ, this dependence is canceled by r_1 and r_2 which are proportional to m_ϕ^{-2} from Eq. (9) (note that dm_γ/dt is independent of m_ϕ in this mass region). As a result, the resonant conversion probability does not depend on m_ϕ.

For $m_\phi \lesssim 10^{-17}$ eV, $g\langle B_0^2\rangle^{1/2}$ at the PRISM/PIXIE constraint reaches the strong coupling limit at resonance epochs. The conversion probabilities in the strong coupling limit are approximated to the identical form to the weak coupling limit as shown in Eqs. (16) and (17). The conversion probability does not depend on ALP mass m_ϕ. Therefore, our constraint can be extended down to $m_\phi \sim 10^{-24}$ eV axions which can play an interesting role in the context of large-scale structure formation [33].

When the ALP mass is $m_\phi < 10^{-14}$, the resonant conversion probability in both limits of weak and strong couplings is proportional to $g^2\langle B_0^2\rangle$. Therefore, PIXIE/PRISM can improve the constraint on $g\langle B_0^2\rangle^{1/2}$ from COBE FIRAS by the ratio $\sqrt{\Delta I_{\rm PRISM}/\Delta I_{\rm FIRAS}} \sim 10^2$ the same as for a larger mass of ALPs, $m_\phi \gtrsim 10^{-14}$.

To close this section we comment on our assumption about the coherent scale of magnetic fields. In our calculations, for simplicity, we have assumed that the coherent scale of magnetic fields is larger than a resonant scale. Here we discuss the validity of this assumption.

Mirizzi, Redondo, and Sigl have studied the condition for this assumption with $m_\phi > m_{\gamma 0}$ [15]. The typical comoving width of a resonance $L_{\rm rc}$ is given by $L_{\rm rc} = (1 + z_r) r \sin 2\theta_r$. Comparing with the comoving coherent scale of magnetic fields, $L_{\rm Mc}$, they showed that the condition of $L_{\rm Mc} > L_{\rm rc}$ is valid when the coupling $g\langle B_0^2\rangle^{1/2}$ satisfies

$$g\langle B_0^2\rangle^{1/2} < 0.06 \left(\frac{m_\phi}{10^{-12}\ {\rm eV}}\right)^{1/3} \times \left(\frac{T_0}{\omega}\right)\left(\frac{L_{\rm Mc}}{1\ {\rm Mpc}}\right)\ {\rm GeV}^{-1}\ {\rm nG}. \quad (21)$$

Our constraint meets this condition with the comoving coherent scale $L_{\rm Mc} \gtrsim 1$ Mpc.

We can also check the validity of the assumption for $m_\phi < m_{\gamma 0}$. Although resonances occur twice at z_1 and z_2, the lower-redshift resonance has a typical comoving width $L_{2c} = (1 + z_2) r_2 \sin 2\theta_2$ larger than the higher-redshift resonance ($z_1 > z_2$). For CMB frequency $4 < \omega/T_0 < 10$, we get the fitting formula of r_2 as

$$r_2 \approx 5.7 \times 10^{-7} \left(\frac{m_\phi}{10^{-14}\ {\rm eV}}\right)^2 \left(-2 + \frac{\omega}{T_0}\right)^4 {\rm Mpc}. \quad (22)$$

Figure 1 shows $z_2 < 500$. Therefore, the condition $L_{\rm Mc} > L_{2c}$ for $4 < \omega/T_0 < 10$ is achieved when the comoving coherent scale of magnetic fields satisfies

$$L_{\rm Mc} > 1.16 \left(\frac{m_\phi}{10^{-14}\ {\rm eV}}\right)^2 {\rm Mpc}, \quad (23)$$

where we used $L_{\rm Mc} > (1 + z_2) r_2$ with $z_2 < 500$ and $\omega/T < 10$. As the ALP mass decreases, our constraint is valid for small-scale magnetic fields. As the ALP mass decreases, our constraint is valid for small-scale magnetic fields, such as those expected to be produced in the QCD or electroweak phase transitions ($L_M c \sim 100$ pc–10 kpc) [48,49].

IV. CONCLUSION

In this paper, we have studied resonant conversions from CMB photons to small-mass ALPs with primordial magnetic fields. Resonant conversions of CMB photons to such small-mass ALPs occur due to plasma effects in the dark age. These resonant conversions can produce observable CMB distortions. We have evaluated the resonant conversion probability between CMB photons and ALPs, following the method of Ref. [15]. In particular, we have focused on low-mass ALPs, $m_\phi < 10^{-10}$ eV. Depending on CMB frequency, CMB photons suffer multiple resonant conversions to such low-mass ALPs.

We have shown that the resonant conversions create a frequency-independent deficit distortion. The frequency spectrum of the distortions due to resonant conversions is different from the distortions due to the energy releases in the early Universe: μ and y distortions and the intermediate distortions between them. Therefore, one can distinguish the distortions due to resonant conversions from these other types.

Using COBE FIRAS bound on the possible CMB distortions from the blackbody spectrum, we have obtained the upper limit on $g\langle B_0^2\rangle^{1/2}$, where g and $\langle B_0^2\rangle^{1/2}$ are the photon-ALP coupling constant and the averaged primordial magnetic field strength at the present epoch, respectively. Our limit is $g\langle B_0^2\rangle^{1/2} \lesssim 10^{-14}\ {\rm GeV}^{-1}\ {\rm nG}$ for $m_\phi \lesssim 10^{-14}$ eV at the CMB frequency $\omega = 4T_0$. We have found that the COBE constraint requires fine-tuned $g\langle B_0^2\rangle^{1/2}$ for $10^{-14}\ {\rm eV} \lesssim m_\phi \lesssim 4 \times 10^{-13}$ eV. This means that ALPs in

this mass region with nonzero photon coupling are effectively ruled out.

We have also evaluated the constraint expected from PIXIE/PRISM; one of whose goals is to measure the CMB frequency spectrum precisely. Compared with COBE FIRAS, PIXIE/PRISM can improve the constraint on $g\langle B_0^2\rangle^{1/2}$ by the ratio of PIXIE/PRISM's CMB distortion sensitivity to COBE FIRAS's one. Accordingly, the PIXIE/PRISM constraint is $g\langle B_0^2\rangle^{1/2} \lesssim 10^{-16}\ \mathrm{GeV}^{-1}\ \mathrm{nG}$ for $m_\phi \lesssim 10^{-14}$ eV at the CMB frequency $\omega = 4T_0$.

The resonant conversion creates the deficit distortion. This fact means that the effective temperature of residual free electron gas, which is thermally equivalent with CMB temperature before the resonant conversion, becomes higher than the effective CMB temperature after the conversion. As a result, in order to recover the thermal equilibrium state, electrons with high momenta cool by Compton scatterings and ones with low momenta absorb CMB photons. This leads to free-free emission and an additional y distortion, whose signature can appear on the CMB spectrum at low frequencies (less than 1 GHz). We will address this issue in the near future.

The current direct constraint on the photon-ALP coupling for small mass is $g \lesssim 10^{-10}\ \mathrm{GeV}^{-1}$ for $m_\varphi \lesssim 0.01$ eV [18]. Our constraint is to the product of the photon-ALP coupling constant g and the magnetic field strength $\langle B_0^2\rangle^{1/2}$. The constraint on $g\langle B_0^2\rangle^{1/2}$ has been also derived from studying the effect of photon-ALP conversions on CMB polarization [50]. Our result shows that COBE FIRAS constraint is comparable with this bound and PIXIE/PRISM can provide the better bound. Recently, the limit similar to the PIXIE/PRISM constraint, $g\langle B_0^2\rangle^{1/2} \lesssim 10^{-16}\ \mathrm{GeV}^{-1}\ \mathrm{nG}$, has been suggested as due to the conversion *from* the axionic dark radiation *to* CMB photons [51]. However, our work relies on the reverse process, which does not require the prior production of axionic dark radiation. Therefore PIXIE/PRISM can give the more robust constraint.

As for primordial magnetic fields, the upper bounds on primordial magnetic fields are provided by observations of CMB anisotropies [52,53] and large-scale structures [54,55]. The constraint on comoving magnetic field strength with the 1 Mpc coherent scale is below several nano Gauss. Therefore, if primordial magnetic fields are detected with the upper limit strength, the PIXIE/PRISM limit can give a stronger constraint on the photon-ALP coupling g stronger by roughly 5 orders of magnitude compared to the present limit for small-ALP mass, $m_\phi < 10^{-14}$ eV.[2]

[2]If the ALP is extremely light, $m_\varphi \lesssim 10^{-28}$ eV, then the photon coupling leads to cosmological birefringence (e.g. [56]) and causes rotation of CMB polarization. Limits from WMAP9 [57] translate to constraints on g of a similar order of magnitude to those obtainable by PIXIE/PRISM for intermediate-scale axion decay constants $f_a \approx 10^{12}$ GeV. Planck polarization results should improve this further.

On the other hand, if in the future the existence of small-mass ALPs were confirmed, for example by direct detection [58,59], and the photon-ALP coupling constant was measured, then the constraint of PIXIE/PRISM constrains primordial magnetic fields. The measurement of CMB distortions by PIXIE/PRISM can then give the stronger constraint on the primordial magnetic fields than other current upper limits.

APPENDIX: RESONANT CONVERSION PROBABILITY IN THE WEAK AND STRONG COUPLING LIMITS

Depending on the ALP mass, we have obtained the analytical approximations of the resonant conversion probability in the weak coupling limit, $m_\phi^2 > gB\omega$, and the strong coupling limit, $m_\phi^2 < gB\omega$ in Sec. II. In particular for $m_\phi < 10^{-14}$ eV, these forms are identical as shown in Eqs. (16) and (17). In this Appendix, we derive these approximate forms in the limits of weak coupling (WC) and of strong coupling (SC).

In both limits, the mixing angle in vacuum, Eq. (2), is approximated by

$$\cos 2\theta_{\mathrm{v}} \approx \begin{cases} 1 - \frac{1}{2}\left(\frac{2gB\omega}{m_\phi^2}\right)^2 & \text{WC limit,} \\ \frac{m_\phi^2}{2gB\omega} & \text{SC limit,} \end{cases} \tag{A1}$$

$$\sin 2\theta_{\mathrm{v}} \approx \begin{cases} \frac{2gB\omega}{m_\phi^2} & \text{WC limit,} \\ 1 - \left(\frac{m_\phi^2}{2gB\omega}\right)^2 & \text{SC limit.} \end{cases} \tag{A2}$$

The wave number of photon-ALP oscillations induced by this mixing angle is expressed in these limits as

$$k \approx \begin{cases} \frac{m_\phi^2}{2\omega} & \text{WC limit,} \\ gB & \text{SC limit.} \end{cases} \tag{A3}$$

Because of cosmic plasma effects, the effective photon mass plays a role. The effective photon mass modifies the mixing angle. The level crossing probability is given by Eq. (8). In this paper, we focus on the limit of nonadiabatic resonance, $p \sim 1$. Therefore, the level crossing probability can be expanded as Eq. (11). Accordingly, using Eqs. (A2) and (A3), we can approximate p in both limits of the weak and strong coupling to

$$1 - p \approx \begin{cases} \pi r\omega g^2 B^2/m_\phi^2 & \text{WC limit,} \\ \pi r\omega g^2 B^2/m_\phi^2 & \text{SC limit.} \end{cases} \tag{A4}$$

In both limits, the level crossing probabilities are identical.

For $m_\phi < 10^{-14}$ eV, the double resonant conversion for CMB photons with $\omega > 4T_0$ happens. The double resonant conversion probability is given by

$$P \approx \frac{1}{2} + \left(p_1(1-p_2) + p_2(1-p_1) - \frac{1}{2} \right) \cos 2\theta_p \cos 2\tilde{\theta}_0. \tag{A5}$$

Let us evaluate the double resonant conversion probability with $\cos 2\theta_p = -1$. When the ALP mass is $m_\phi < 10^{-14}$ eV, $m_{\gamma 0} \gg m_\phi$ is satisfied as shown in Fig. 1. Hence the effective mixing angle $\cos 2\tilde{\theta}_0$ at the detection point ($z = 0$) can be approximated by

$$\begin{aligned} \cos 2\tilde{\theta}_0 &\approx -1 + \frac{1}{2}\frac{\sin^2 2\theta_{\rm v}}{\xi^2} \\ &\approx \begin{cases} -1 + \frac{1}{2}\left(\frac{m_\phi}{m_{\gamma 0}}\right)^4 \left(\frac{2gB_0\omega}{m_\phi^2}\right)^2 & \text{WC limit}, \\ 1 + \frac{1}{2}\left(\frac{2gB_0\omega}{m_{\gamma 0}^2}\right)^2 & \text{SC limit}, \end{cases} \end{aligned} \tag{A6}$$

where B_0 is the comoving magnetic field strength. The current constraints on g and B_0 are $g \lesssim 10^{-10}$ GeV^{-1} and $B \lesssim 1$ nG. These constraints suggest that $m_{\gamma 0}^2 \gg gB\omega$ for $\omega < 10T_0$. Therefore, we can assume $\cos 2\tilde{\theta}_0 \approx -1$ in both limits.

Plugging Eqs. (A4) and (A5) into Eq. (A5), we obtain in the limits of weak and of strong couplings

$$P \approx \pi\omega \frac{g^2 B_0^2}{m_\phi^2} [r_1(1+z_1)^5 + r_2(1+z_2)^5], \tag{A7}$$

where we use $B_i = B_0(1+z_i)^2$ and $\omega_i = \omega(1+z_i)$ with the subscript i denoting 1 and 2. Equation (A7) corresponds to Eqs. (16) and (17).

ACKNOWLEDGMENTS

We thank Jens Chlubas for useful comments. H. T. is supported by the DOE. The research of J. S. has been supported at IAP by the ERC Project No. 267117 (DARK) hosted by Université Pierre et Marie Curie–Paris 6 and at JHU by NSF Grant No. OIA-1124403. The research of D. J. E. M. was supported by Perimeter Institute for Theoretical Physics. Research at Perimeter Institute is supported by the Government of Canada through Industry Canada and by the Province of Ontario through the Ministry of Researc\h and Innovation.

[1] R. D. Peccei and H. R. Quinn, Phys. Rev. Lett. **38**, 1440 (1977).
[2] S. Weinberg, Phys. Rev. Lett. **40**, 223 (1978).
[3] F. Wilczek, Phys. Rev. Lett. **40**, 279 (1978).
[4] E. Witten, Phys. Lett. **149B** 351 (1984).
[5] P. Svrcek and E. Witten, J. High Energy Phys. 06 (**2006**) 051.
[6] A. Arvanitaki, S. Dimopoulos, S. Dubovsky, N. Kaloper, and J. March-Russell, Phys. Rev. D **81**, 123530 (2010).
[7] B. S. Acharya, K. Bobkov, and P. Kumar, J. High Energy Phys. 11 (**2010**) 105.
[8] M. Cicoli, M. Goodsell, and A. Ringwald, J. High Energy Phys. 10 (**2012**) 146.
[9] A. Neronov and I. Vovk, Science **328**, 73 (2010).
[10] F. Tavecchio, G. Ghisellini, L. Foschini, G. Bonnoli, G. Ghirlanda, and P. Coppi, Mon. Not. R. Astron. Soc. **406**, L70 (2010).
[11] A. Kandus, K. E. Kunze, and C. G. Tsagas, Phys. Rep. **505**, 1 (2011).
[12] L. M. Widrow, D. Ryu, D. R. G. Schleicher, K. Subramanian, C. G. Tsagas, and R. A. Treumann, Space Sci. Rev. **166**, 37 (2012).
[13] R. Durrer and A. Neronov, Astron. Astrophys. Rev. **21**, 62 (2013).
[14] T. Yanagida and M. Yoshimura, Phys. Lett. B **202**, 301 (1988).
[15] A. Mirizzi, J. Redondo, and G. Sigl, J. Cosmol. Astropart. Phys. 08 (**2009**) 001.
[16] J. C. Mather *et al.*, Astrophys. J. **420**, 439 (1994).
[17] D. J. Fixsen, E. S. Cheng, J. M. Gales, J. C. Mather, R. A. Shafer, and E. L. Wright, Astrophys. J. **473**, 576 (1996).
[18] S. Andriamonje *et al.* (CAST Collaboration), J. Cosmol. Astropart. Phys. 04 (**2007**) 010.
[19] G. G. Raffelt, Lect. Notes Phys. **741**, 51 (2008).
[20] A. Friedland, M. Giannotti, and M. Wise, Phys. Rev. Lett. **110**, 061101 (2013).
[21] A. Kogut *et al.*, J. Cosmol. Astropart. Phys. 07 (**2011**) 025.
[22] P. Andre *et al.* (PRISM Collaboration), arXiv:1306.2259.
[23] Y. B. Zeldovich and R. A. Sunyaev, Astrophys. Space Sci. **4**, 301 (1969).
[24] R. A. Sunyaev and Y. B. Zeldovich, Astrophys. Space Sci. **7**, 20 (1970).
[25] L. Danse and G. de Zotti, Riv. Nuovo Cimento Soc. Ital. Fis. **7**, 277 (1977).
[26] C. Burigana, L. Danese, and G. de Zotti, Astron. Astrophys. **246**, 49 (1991).
[27] W. Hu and J. Silk, Phys. Rev. D **48**, 485 (1993).
[28] J. Chluba and R. A. Sunyaev, Mon. Not. R. Astron. Soc. **419**, 1294 (2012).
[29] R. A. Sunyaev and R. Khatri, Int. J. Mod. Phys. D **22**, 1330014 (2013).
[30] W. Hu, R. Barkana, and A. Gruzinov, Phys. Rev. Lett. **85**, 1158 (2000).
[31] L. Amendola and R. Barbieri, Phys. Lett. B **642**, 192 (2006).

[32] D. J. E. Marsh, D. Grin, R. Hlozek, and P. G. Ferreira, Phys. Rev. D **87**, 121701(R) (2013).
[33] D. J. E. Marsh and J. Silk, arXiv:1307.1705.
[34] A. Arvanitaki and S. Dubovsky, Phys. Rev. D **83**, 044026 (2011).
[35] G. Raffelt and L. Stodolsky, Phys. Rev. D **37**, 1237 (1988).
[36] A. Mirizzi, J. Redondo, and G. Sigl, J. Cosmol. Astropart. Phys. 03 (**2009**) 026.
[37] M. Born and E. Wolf, *Principles of Optics* (Pergamon, New York, 1980), pp. 691–692.
[38] G. Hinshaw *et al.* (WMAP Collaboration), Astrophys. J. Suppl. Ser. **208**, 19 (2013).
[39] S. Seager, D. D. Sasselov, and D. Scott, Astrophys. J. **523**, L1 (1999).
[40] G. G. Raffelt, *Stars as Laboratories for Fundamental Physics: The Astrophysics of Neutrinos, Axions, and Other Weakly Interacting Particles* (Chicago University, Chicago, 1996).
[41] L. Wolfenstein, Phys. Rev. D **17**, 2369 (1978).
[42] S. P. Mikheev and A. Y. Smirnov, Yad. Fiz. **42**, 1441 (1985) [Sov. J. Nucl. Phys. **42**, 913 (1985)].
[43] S. J. Parke, Phys. Rev. Lett. **57**, 1275 (1986).
[44] D. J. Fixsen, Astrophys. J. **707**, 916 (2009).
[45] A. F. Illarionov and R. A. Siuniaev, Sov. Astron. **18**, 691 (1975).
[46] R. Khatri and R. A. Sunyaev, J. Cosmol. Astropart. Phys. 09 (**2012**) 016.
[47] J. Chluba, Mon. Not. R. Astron. Soc. **434**, 352 (2013).
[48] R. Banerjee and K. Jedamzik, Phys. Rev. Lett. **91**, 251301 (2003); , Phys. Rev. Lett. **93**, 179901(E) (2004).
[49] T. Kahniashvili, A. G. Tevzadze, A. Brandenburg, and A. Neronov, Phys. Rev. D **87**, 083007 (2013).
[50] P. Tiwari, Phys. Rev. D **86**, 115025 (2012).
[51] T. Higaki, K. Nakayama, and F. Takahashi, J. Cosmol. Astropart. Phys. 09 (**2013**) 030.
[52] D. Paoletti and F. Finelli, Phys. Lett. B **726**, 45 (2013).
[53] P. A. R. Ade *et al.* (Planck Collaboration), arXiv:1303.5076.
[54] K. L. Pandey and S. K. Sethi, Astrophys. J. **762**, 15 (2013).
[55] T. Kahniashvili, Y. Maravin, A. Natarajan, N. Battaglia, and A. G. Tevzadze, Astrophys. J. **770**, 47 (2013).
[56] S. M. Carroll, G. B. Field, and R. Jackiw, Phys. Rev. D **41**, 1231 (1990).
[57] G. Hinshaw *et al.* (WMAP Collaboration), Astrophys. J. Suppl. Ser. **208**, 19 (2013).
[58] J. Jaeckel and A. Ringwald, Annu. Rev. Nucl. Part. Sci. **60**, 405 (2010).
[59] A. Ringwald, arXiv:1209.2299.